Available online at www.sciencedirect.com
SCIENCE DIRECT®

Journal of the European Ceramic Society 24 (2004) 2285–2292
www.elsevier.com/locate/jeurceramsoc

Initial sintering stage pore growth mechanism applied to the manufacture of ceramic membrane supports

Cavus Falamaki*, Mahdi Shafiee Afarani, Alireza Aghaie

Ceramics Department, Materials and Energy Research Center, PO Box 14155-4777, Tehran, Iran

Received 5 March 2003; received in revised form 21 June 2003; accepted 6 July 2003

Abstract

Initial sintering stage pore growth mechanism has been applied to the manufacture of alumina and zircon membrane supports formed by uniaxial compaction. The effect of sintering temperature (1200–1500 °C) on density, porosity, surface area, permeability, mean flow pore size, mesopores mean radius (<7 nm) and tortuosity has been investigated. A transition zone has been determined at the end of which permeability reaches a maximal value. Alumina and zircon samples possessed a reasonable flexural strength at the latter point. The transition zone is accompanied with a decrease in tortuosity for both materials. The trend of tortuosity change after the transition zone strongly depended on the shrinkage behavior of the samples.

Keywords: Al_2O_3; Membranes; Microstructure-final; Silicates; Sintering

1. Introduction

The science of ceramic membrane manufacture has undergone rapid growth during the last two decades. The interest in ceramic membranes has increased concurrently with new processes and new applications. The rapidly changing environmental legislation in the use of chemicals and reagents also makes them very attractive.[1]

Although a huge amount of information about the manufacture of micro to nano-filter ceramic layers has been disclosed in the open literature, the latter is relatively lean on information about support layers manufacture. These have a pore size distribution in the range of 0.1–15 μm. Supports with average pore diameters larger than 1 μm are considered as macroparticle filters.[2] Ceramic supports are mainly produced by dry compaction and extrusion forming processes. The macroporous support is further coated by dip coating with different layers with decreasing pore size.[3] Dry compaction of Al_2O_3 for the synthesis of such supports has been investigated by a few numbers of workers.[4,5]

In the industry this route is usually accompanied with the burning out of organic additives to permit pore structure control. Preparation by the extrusion method (Al_2O_3) has been the subject of some recent reports.[6–8] A proper ceramic support should have high permeability, high mechanical strength, sharp pore size maximum[3], and high specific surface area. Therefore, optimization of manufacturing process parameters to achieve these characteristics is a hard challenge.

Such an optimization study for the manufactured supports via the compression route has been neglected in the open literature.

In the production of dense ceramics through initial powder compacts sintering, elimination of pore growth is desired. Pore growth during the early stages of sintering of oxide ceramics is a well-known phenomenon[9] but has been the subject of only a few individual studies.[10–12] However, the evolution of permeability and tortuosity characteristics were not considered. The work of Whittemore and Sipe[10] showed pore growth of alumina was a function of initial powder particle size and compaction pressure. Larger particles (0.3 μm) showed pore growth only at high pressures (50 000 psia), while smaller ones (0.05 μm) needed lower pressures (127 00 psia). Such a dependence of pore growth on the physical properties of the initial compact was further investigated by Zheng and Reed.[11] They elucidated the effect of pore growth/elimination on the final sintered density of alumina compacts. They presented a critical ratio

* Corresponding author. Fax: +98-0262-6221-888.
E-mail address: c-falamaki@merc.ac.ir (C. Falamaki).

0955-2219/$ - see front matter © 2003 Published by Elsevier Ltd.
doi:10.1016/S0955-2219(03)00643-5

(maximum pore size of initial compact over mean particle size of initial powder) for the determination of the possible elimination of pores during the early and intermediate stages of sintering. Permeance and tortuosity characteristics were not investigated.

The present study aims at investigating the evolution of typical membrane characteristics (like permeability and tortuosity) of Al_2O_3 and $ZrSiO_4$ membranes with the sintering temperature applying the dry compaction procedure. The main hint applied had been the implementation of the initial sintering stage pore growth mechanism to promote pore shape and connectivity evolution to obtain high permeability and high flexural strength final products. No organic/inorganic additive for the production of porosity has been applied. Although Al_2O_3 and $ZrSiO_4$ raw materials were different in nature, during initial sintering they showed a common trend in many aspects. Such an investigation is novel and its outcomes may be used to design ceramic support manufacturing processes.

2. Experimental procedure

An alumina molding powder (Martinswerke, KMS-96) with an average granule size of 160 μm was used. Its typical analysis was Al_2O_3 96.00 wt.%, Na_2O 0.20 wt.%, K_2O 0.05 wt.%, SiO_2 3.00 wt.% and MgO 0.10 wt.%. For the zircon powder, Zircosil 5 (95.00 wt.% content having particles smaller than 1.78 μm) was used. The latter contained 0.492 wt.% Fe, 0.376 wt.% Al and 0.083 wt.% P as impurity.

For the zircon samples, 4 wt.% PVA (0.2 wt.% aqueous solution) was added to the powders before compaction. These powders were aged and gently blended for 48 h at RT. The resulting powder was passed over a 40 mesh screen. The undersieve (<425 μm) agglomerates were used. Alumina granules were pressed without any binder addition. In each case, 1 g of the resulting powders was uniaxially pressed (forming pressure 31.2 MPa) to form disks of a diameter of 20 mm (five samples for each experiment). The resulting green compacts were fired in air atmosphere according to the following sequential heating program: Heating up to 1000 °C with a heating rate of 20 °C min^{-1}, heating up to the sintering temperature with a heating rate of 5 °C min^{-1} and 1 h soaking time. Phase and microstructure analysis was performed using XRD (Siemens, D-500 diffractometer) and SEM (Stereo Scan 360-Leica, Cambridge) techniques. Dry and wet permeability tests are described elsewhere.[5] Paraffin was used as saturation medium to make possible working at lower pressures and avoiding premature sample rupture. The special apparatus used for nitrogen permeability measurements[13] allowed us to cover the whole range from pure Knudsen to pure Poiseuille flow regime for all the samples. Density and porosity were measured according to ASTM C 373-88. Four point flexural strength measurements were performed on $58.4\times4.70\times3.90$ mm^3 rectangular bars with a mechanical testing machine (Instron model 1196). Specific surface area measurements and adsorption isotherm determination were done using a micromeritics apparatus.

3. Results and discussion

A continuous trend of porosity decrease with increasing sintering temperature both for Al_2O_3 and $ZrSiO_4$ supports is shown in Fig. 1. It is observed that for Al_2O_3, porosity's higher than 30% are obtainable only for sintering temperatures lower than 1425 °C. For zircon samples, the latter temperature is 1500 °C. A transition zone in the temperature range of 1350–1400 °C is observed for either case. Within the transition zone, the densification process undergoes acceleration. The former zone may also be observed in the shrinking versus temperature curves (Fig. 2).

Considering the changes of specific surface area with sintering temperature, a sharp decrease is observed both for Al_2O_3 and $ZrSiO_4$ samples within the temperature domain of 1350–1375 and 1350–1400 °C, respectively

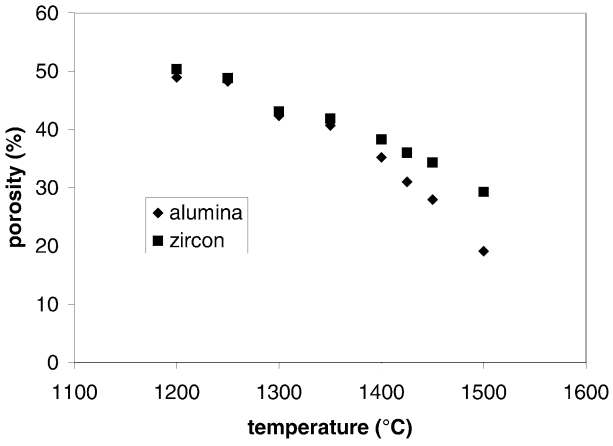

Fig. 1. Porosity versus sintering temperature for the alumina and zircon samples.

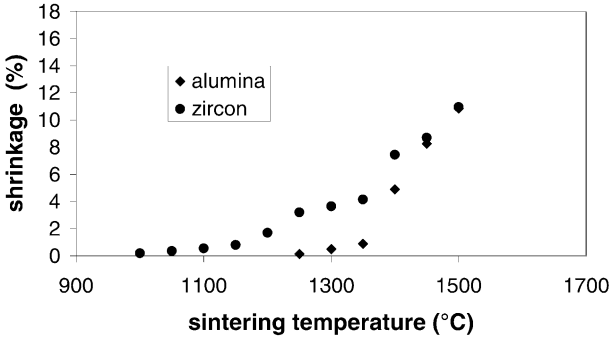

Fig. 2. Shrinkage versus sintering temperature for the alumina and zircon samples.

(Fig. 3a,b). The abrupt change is more pronounced for Al_2O_3. Accordingly, the authors of the present work assign the latter temperature ranges as the more precise "transition zones" cited before for the alumina and zircon samples.

As a membrane support, one of the main characteristics of concern is permeability. The variation of permeability (in the Knudsen flow regime) with sintering temperature is shown in Fig. 4. Considering the Al_2O_3 samples, an interesting behavior may be observed. Up to 1350 °C, the permeability is approximately constant. Just in the transition zone mentioned, a sharp increase in permeability (approximately 1.5× at 1375 °C) is observed. After this temperature a strong continuous decrease in permeability follows. Such a maximum in the permeability versus sintering temperature curve exists for $ZrSiO_4$ samples, although the changes are rather smooth and the maximal permeability is only about 20% more than the initial value. Fig. 5 shows the flexural strength of some of the sintered samples at different temperatures. It is observed that both alumina and zircon samples already posses a reasonable mechanical strength (>20 MPa) at the end of the corresponding transition zones.

It is noteworthy to emphasize that pore size distributions evaluated using wet permeability tests might be more indicative than mercury porosimetry tests, as the true filtrating pores are concerned. Fig. 6 shows the wet permeability test for the alumina samples sintered at different temperatures. For illustration purposes, the line corresponding to one half the dry gas flow rates for

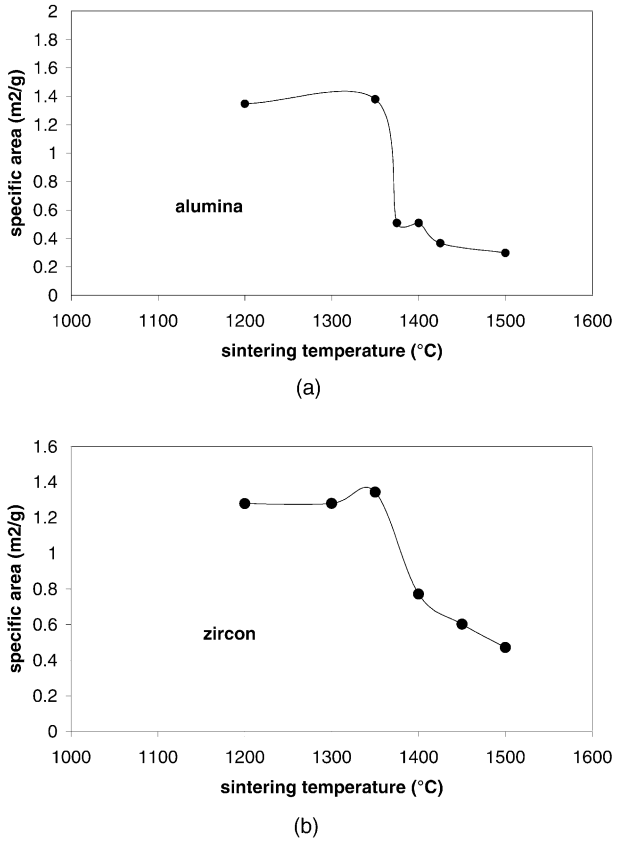

Fig. 3. Specific area as a function of sintering temperature for (a) alumina and (b) zircon samples.

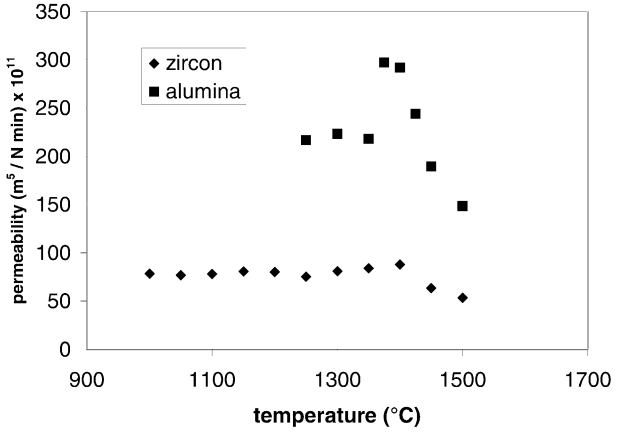

Fig. 4. Permeability (Knudsen flow regime) as a function of sintering temperature for the alumina and zircon samples.

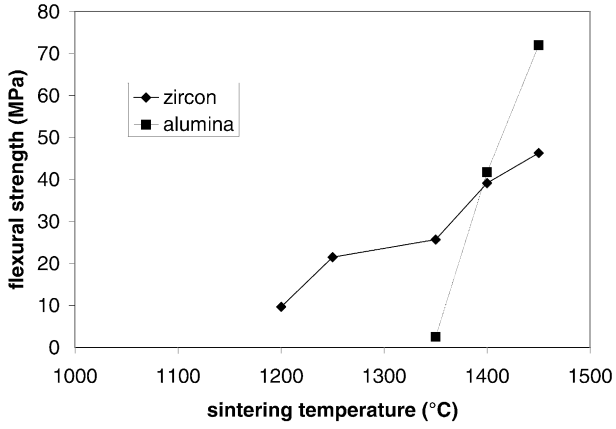

Fig. 5. Flexural strength versus sintering temperature for some of the alumina and zircon samples.

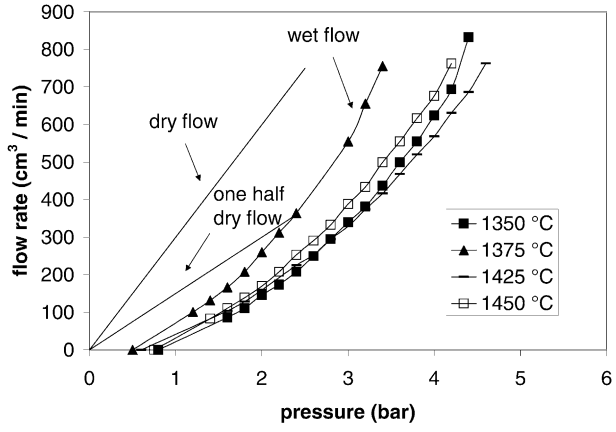

Fig. 6. Nitrogen flow rate versus gas pressure for the wet permeability tests of the alumina samples. The dry and one half dry gas flow rate lines have been drawn for the sample sintered at 1375 °C.

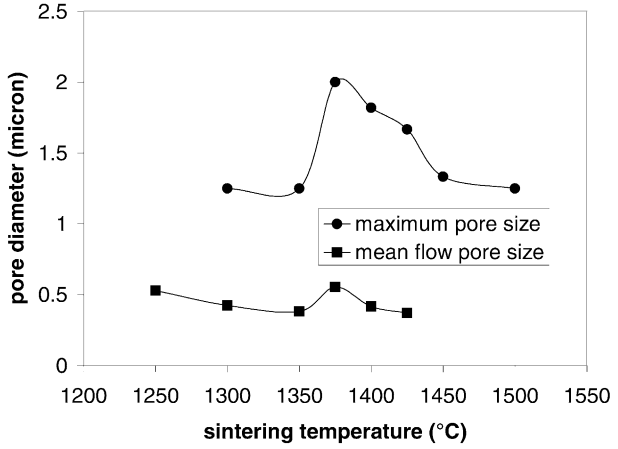

Fig. 7. Maximum and mean flow pore size as a function of sintering temperature for the alumina samples.

the sample sintered at 1375 °C has been drawn. The intersection of the latter with the wet flow curve corresponds to the mean flow pore pressure. The corresponding pore size is the mean flow pore size. Fig. 7 shows the variation of the maximum permeable and mean flow pore diameter with changes of sintering temperature. It should be mentioned that maximum permeable pore size so determined is not always equal to the maximum pore size due to SEM micrographs. This fact has been elucidated by Falamaki et al.[5] It should be emphasized that the initial alumina powder consists of relatively large agglomerates which, upon pressing, do break into particles approximately one order of magnitude smaller. The existence of glassy phase impurities like SiO_2 eventually make the pore growth process take place at lower temperatures. Interestingly, Figs. 7 and 4 resemble each other significantly in that the transition zone is similar (for alumina samples). The same similarity was observed also for the $ZrSiO_4$ supports. Such an increase in the permeability with sintering temperature has been recently reported by Shojai and Maentylae[14] for zirconia samples. They concluded that this phenomenon had been a result of tortuosity decrease and mean pore diameter increase. Tortuosity data were not reported.

The micrographs relating the evolution of the microstructure of Al_2O_3 samples with the increasing sintering temperature are shown in Fig. 8. The initially compact structures of the samples sintered at 1300 and 1350 °C transform into an 'open' structure at 1375 °C. Afterwards the densification process (shrinkage) dominates and at a sintering temperature of 1500 °C, a quite dense and 'closed' microstructure is observed. Thus, the results due to microphotography seem to be in accordance with the results cited above. The micrographs of zircon samples also evidence such a trend, although not

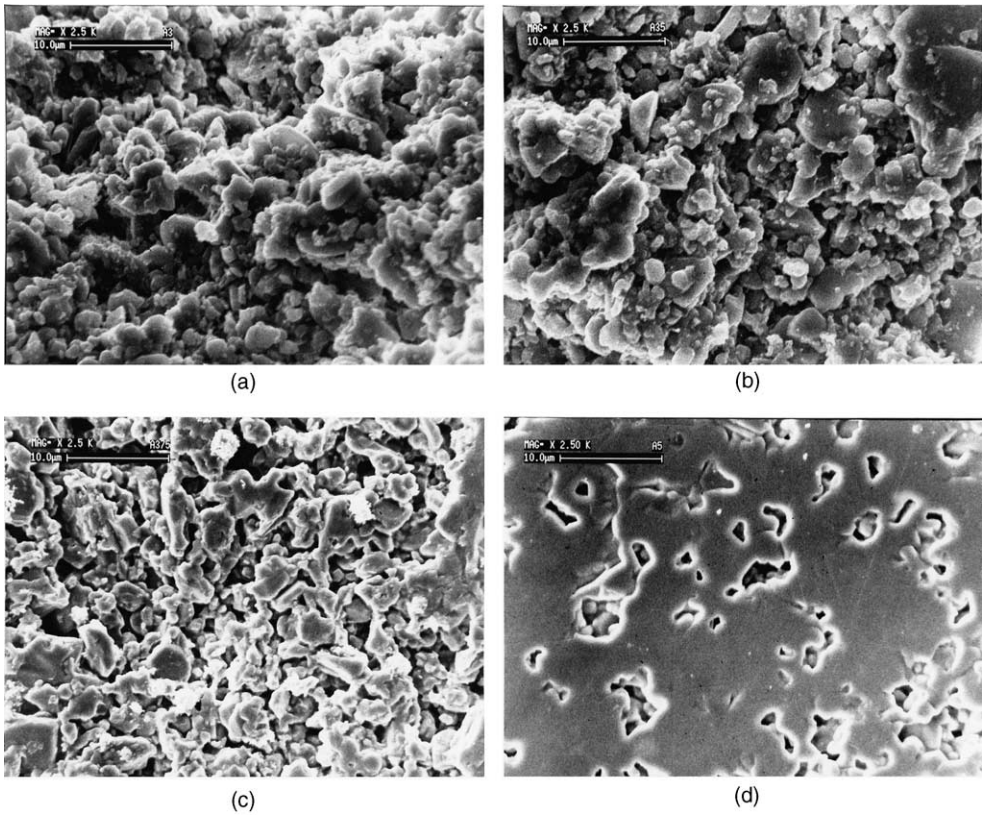

Fig. 8. Microstructure of alumina samples sintered at different temperatures: (a) 1300, (b) 1350, (c) 1375 and (d) 1500 °C.

as distinct for the alumina samples. A relatively open structure is observable at 1400 °C (Fig. 9).

A more accurate average permeable pore size determination was performed using gas permeability data pertaining to pure Knudsen and pure Poiseuille flow regimes. It may be shown that the average pore diameter and tortuosity can be evaluated from the following relations:

$$r = \frac{16 \cdot \eta \cdot (8RT/\pi M)^{0.5} S}{3 \cdot F_k} \quad (1)$$

$$\tau/\varepsilon = \frac{256 \cdot \eta \cdot S}{9 \cdot \pi \cdot MLF_k^2} \quad (2)$$

Where r is the average permeable pore radius (m), η the gas viscosity (kg m^{-1} s^{-1}), R the universal gas constant (J mol^{-1} K^{-1}), T the temperature (K), M the gas molecular weight (kg $mole^{-1}$), S the slope of the permeability versus mean pressure curve in the pure Poiseuille flow region (mole m^{-2} s^{-1} Pa^{-2}), F_k the permeability in the pure Knudsen flow regime (mole m^{-2} s^{-1} Pa^{-1}), τ the tortuosity, ϵ the porosity and L the membrane thickness (m).

Fig. 10 shows the calculated pore diameters for the alumina and zircon samples. Table 1 summarizes the pertaining experimental values of S used in Eqs. (1)–(2).

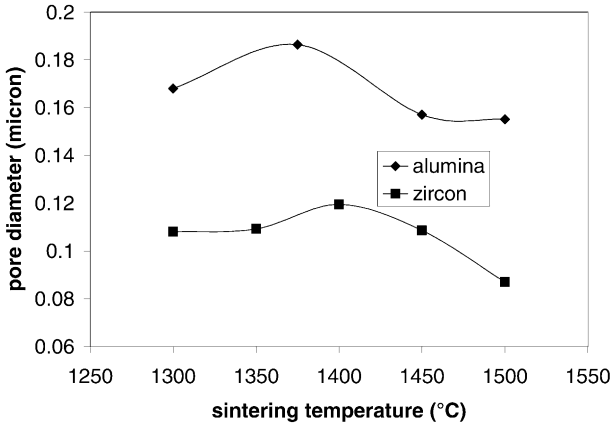

Fig. 10. Calculated pore diameter versus sintering temperature using Eq. (1).

The previous results showing pore growth during the transition regions are confirmed. It is observed that, in the case of alumina, the calculated pore diameters are less than half the values obtained for the mean flow pore size. Actually wet permeation measurements give reliable results only for the bubble point (largest active pores) and not for pore size distribution. The authors of this study have observed a strong dependence of the permeability data on the rate of pressure increase during the wet measurements. During liquid displacement through the pores, a thin layer may remain adhered on

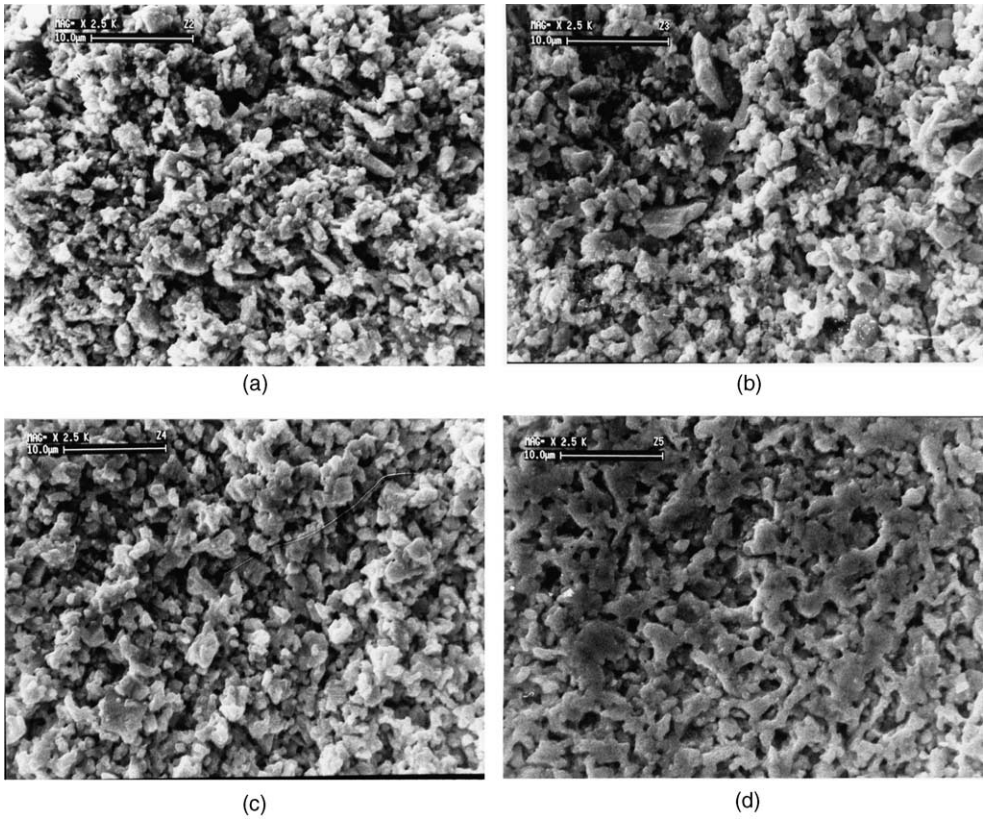

Fig. 9. Microstructures of zircon samples sintered at different temperatures: (a) 1200, (b) 1300, (c) 1400 and (d) 1500 °C.

the walls. This may result in a significant reduction of wall roughness thus affecting gas flow.

Generally, pore growth within the initial stages of sintering may occur by many different mechanisms[10]: surface diffusion, particle size distribution effects, particle coalescence, phase transformation and evaporation/condensation. The result is some kind of particle rearrangement in the initial step of sintering. Some groups of relatively small highly compact aggregates shrink on themselves by particle rearrangement with neck growth, resulting in the growth of irregular voids caused by the separation between the shrinking groups.[15] The abrupt reduction of surface area at the end of the transition region (corresponding to maximum pore diameter) might be related to the elimination of such small entities having high surface areas.

Some insight into the aforesaid process may be gained following the mesopores (2–50 nm) size evolution. Actually, the pore growth considered up to this point concerned the 'macropores' (>50 nm). Usually, ceramic powder compacts show a bimodal (at least) pore size distribution. In the case of samples having a prevailing pore volume due to macropores, the mesopores could actually be considered as funnel shaped corners between large particles. These are apt to condense vapors. Using the BET technique to draw the isotherms of nitrogen adsorption for the Al_2O_3 and $ZrSiO_4$ samples, it is possible to evaluate the mesopore size distribution at each sintering temperature. As it will be shown later, the average mesopore size of the alumina and zircon samples under study had been less than 7.5 nm. The latter corresponds to pressures higher than 2000 atm, which would eventually result in the collapse of the samples, if mercury porosimetry is used. On the other hand, 7.5 nm is a limiting figure for most commercial mercury porosimeter instruments.[16] Thus the use of BET technique is highly justified. Fig. 11 shows the isotherms for the Al_2O_3 samples. It is observed that the samples exhibit adsorbed layer prior to the condensation of nitrogen. Considering a Maxwellian pore volume distribution, the volume occupied by the adsorbate $V(p)$ may be calculated by the following equation:

$$V(p) = V_s\left(\left[1 - \left(1 + \frac{r}{r_0}\right)\exp\left(-\frac{r}{r_0}\right)\right] + \frac{2t}{r_0}\left[\exp\left(-\frac{r}{r_0)}\right) - \exp\left(-\frac{r_{\max}}{r_0}\right)\right]\right) \quad (3)$$

Where V_s is the total pore volume ($cm^3\ g^{-1}$), r_0 a constant (nm), r the pore radius (nm), r_{max} the threshold

Table 1
Values of S used in Eqs. (1)–(2)

Sintering temperature (°C)	Alumina samples$\times 10^{12}$ (mol $m^{-2}\ s^{-1}\ Pa^{-2}$)	Zircon samples$\times 10^{12}$ (mole $m^{-2}\ s^{-1}\ Pa^{-2}$)
1300	9.9	2.4
1350	–	2.6
1375	13.3	–
1400	–	3.3
1450	5.1	2.1
1500	7.3	1.2

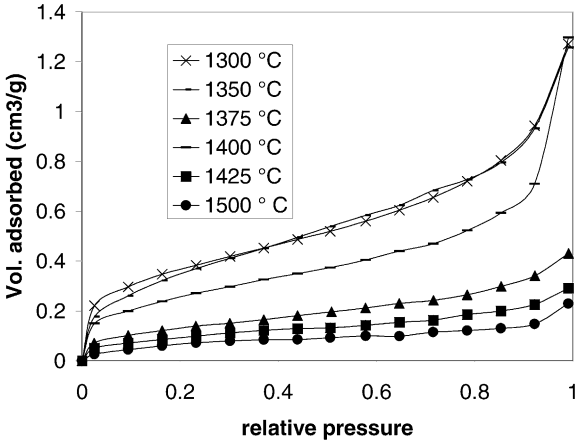

Fig. 11. Nitrogen adsorption isotherms of the alumina samples sintered at different temperatures.

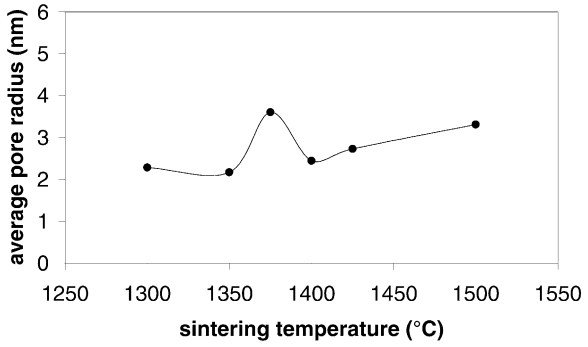

Fig. 12. Mesopore radius evolution as a function of sintering temperature for the alumina samples.

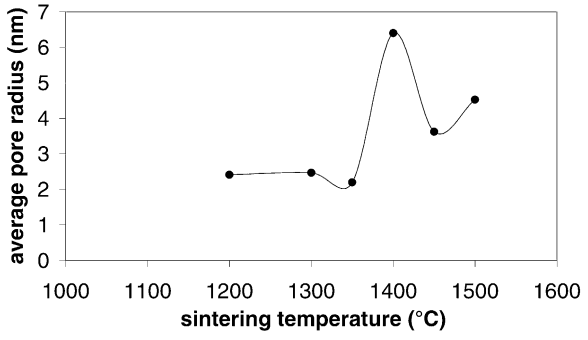

Fig. 13. Mesopore radius evolution as a function of sintering temperature for the zircon samples.

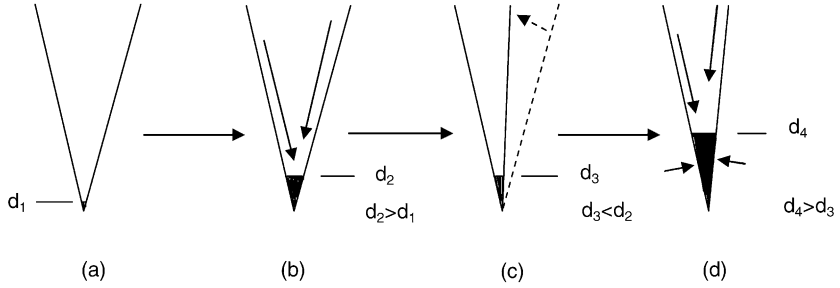

Fig. 14. Scheme of mesopore evolution: (a) Initial funnel tip diameter (d_1) before the transition zone (b) Enlarged diameter due to filling with the nearby shrinking groups (end of the transition zone) (c) Diameter decrease due to shrinkage (d) Diameter increase due to material diffusion (surface and volume diffusion has been shown) during the densification stage.

pore radius (nm) and t the statistical thickness of the adsorbed layer (nm).

Employing the statistical model of Halsy for the evaluation of t[16] in Eq. (3), the mesopore size distribution could be obtained. Figs. 12–13 show the evolution of the average mesoporous radius for the Al_2O_3 and $ZrSiO_4$ samples, respectively. Both seem to follow a unique trend. At low sintering temperatures the pore size remains approximately constant. A sharp increase occurs at the transition zones already defined. Then, at higher temperatures initially the pore size reduces and then begins to increase. Such a behavior has not been reported earlier. These observations can be explained according to the following scheme: During the transition zone, funnel shaped mesopores are filled with the nearby shrinking groups as discussed before. The result is an enlargement of funnel tip diameter (Fig. 14a). After the transition zone, the tip diameter is first sharply decreased due to significant shrinkage (Fig. 14b). Further densification at higher sintering temperatures enlarges the mesopores again by the tip filling mechanism (Fig. 14c).

An important aspect of the microstructure evolution concerning the membrane behavior of the samples, is the variation of the tortuosity with sintering temperature. The irregular shape of macropores pores and their connectivity is usually lumped into one single parameter called tortuosity (τ).

Fig. 15 shows the variation of τ for each series of samples. It is observed that pore growth during the transition region is accompanied by a decrease in tortuosity, both for alumina and zircon samples. After the transition region, the tortuosity of alumina samples continues to decrease up to 1450 °C and afterwards increase slightly. For the zircon samples tortuosity increases after the transition region up to 1450 °C and decreases slightly afterwards. Such trends have not been reported before.

It is generally assumed that tortuosity originates from the increasing length of the diffusion path for a gas molecule in a porous medium compared to a straight capillary. Tortuosity combines two main factors, S_s the pore shape factor and S_τ, the tortuosity factor ($\tau = S_s.S_\tau$). During the very first stage of sintering, a minority of high surface area particles are eventually distributed among the larger ones. Increasing the sintering temperature, these particles are transferred to the surface of the larger particles leaving a new pore with a new shape.

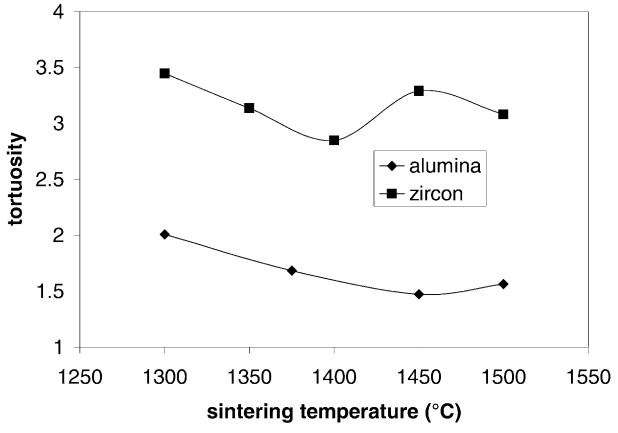

Fig. 15. Calculated tortuosity versus sintering temperature using Eq. (2).

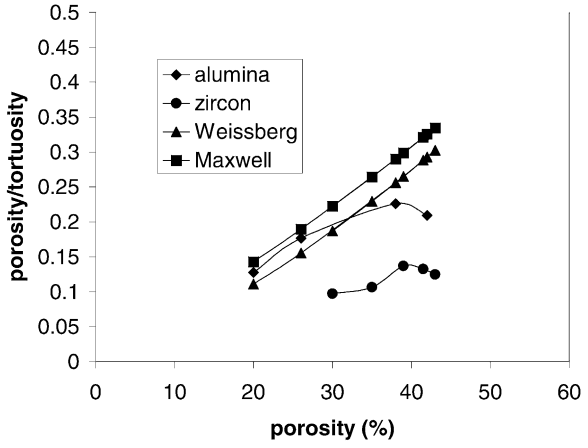

Fig. 16. Weakness of theoretical models in relating tortuosity to porosity for the sintered samples of this study (Maxwell model: $\tau = 1 + 0.5\ln(1-\varepsilon)$, Weissberg model : $\tau = 1 - 0.5\ln\varepsilon$).

During this stage, shrinkage is minimal and porosity decreases only slightly. In other words, the main factor changing is S_s. Shrinkage due to higher sintering temperatures, which may involve many diffusion mechanisms, eliminates pore connectivity to a large extent. This is a competing process, which results in higher S_τ values. As sintering proceeds, i.e. during the intermediate stages ($\epsilon > 20\%$), densification may again result in change of pore shapes in such a way that S_s decreases. According to Fig. 2, alumina samples undergo significant shrinkage only after 1450 °C (ca. 9%). In other words, increase in S_τ may counterbalance the decrease in S_s due to pore shape decrease only after the latter temperature. Referring again to Fig. 2, it is clear that zircon samples undergo significant shrinkage only after 1400 °C. Then, using the same reasoning, the minimum for the tortuosity observed at this temperature for the zircon samples can be similarly explained.

Existing theoretical models[17] are not able to relate correctly tortuosity to porosity for the systems under study (see Fig. 16). The evolution of the void labyrinth structure in terms of pore size, shape and tortuosity during sintering of ceramics is a major topic worth of further study.

4. Conclusion

The evolution of permeable alumina and zircon green compact physical properties with sintering temperature have been investigated. Regarding microstructure and membrane characteristics, a transition zone could be observed for both:

1. The transition zone is accompanied with an increase in mean flow pore diameter and permeability and decrease in tortuosity. However, tortuosity may further decrease after the transition zone if shrinkage is negligible.
2. The mesopores (<7 nm) undergo an abrupt increase in size at the point corresponding to maximum permeability within the transition zone. This may result in less internal roughness and less resistance to gas flow, thus affecting positively the permeability.
3. Both alumina and zircon samples had a flexural strength higher than 20 MPa at the end of the transition zone (point of maximum permeability). Therefore the point of maximum permeabilty coincides with a reasonable mechanical strength for using the sintered samples as membrane supports.
4. The outcomes of this study might be used for the design of membrane/catalyst supports.

References

1. Chan, K. K. and Brownstein, A. M., Ceramic membranes-growth prospects and opportunities. *Ceramic Bulletin*, 1991, **70**, 703–707.
2. Morgart, J. R., Filson, J. L., Peters, J. J. and Bhave, R. R., Bacteria removal by ceramic microfiltration, US Patent 5 242 595, 1993.
3. Luyten, J., Cooymans, J., Adriansen, W. and Leysen, R., Alternative process routes for better ceramic supports. *Industrial Ceramics*, 2000, **20**, 29–31.
4. Luyten, J., Cooymans, J. and Leysen, R. Shaping of a RBAO-membrane support, In *Key Engineering Materials*, 1997, vols. 132-136, pp. 1691-1694.
5. Falamaki, C., Aghaie, R. and Ardestani, N. R., RBAO membranes/catalyst supports with enhanced permeability. *J. Eur. Ceram. Soc.*, 2001, **21**, 2267–2274.
6. Ananthakumar, S., Menon, A. R. R., Pabhakaran, K. and Warrier, K. G. K., Rheology and packing characteristics of alumina extrusion bohemite gel as a binder. *Ceramics International*, 2001, **27**, 231–237.
7. Shkrabina, R. A., Boneckamp, R. A., Pax, P., Veringa, H. and Ismagilov, Z. R., Porous structure of alumina ceramic supports for gas separation membranes, I. Preparation and study of the extrusion masses. *React. Kinet. Catal. Lett.*, 1995, **54**, 181–191.
8. Shkrabina, R. A., Boneckamp, R. A., Pax, P., Veringa, H. and Ismagilov, Z. R., Porous structure of alumina ceramic supports for gas separation membranes, II. Study of porous structure of ceramic composition. *React. Kinet. Catal. Lett.*, 1995, **54**, 193–201.
9. German, R. M., *Sintering Theory and Practice*. John Wiley and Sons, 1996.
10. Whittemore, O. J. and Sipe, J. J., Pore growth during the initial stages of sintering ceramics. *Powder Technology*, 1974, **9**, 159–164.
11. Zheng, J. and Reed, J. S., Effects of particle packing characteristics on solid-state sintering. *J. Am. Ceram. Soc.*, 1989, **72**, 810–817.
12. Zheng, J. and Reed, J. S., The different roles of forming and sintering on densification of powder compacts. *Am. Ceram. Soc. Bull.*, 1992, **71**(9), 1410–1416.
13. Falamaki, C., Aghaie, A. and Ardestani, N. R., Iranian Patent 26 446, 2000.
14. Shojai, F. and Maentylae, T. A., Effect of sintering temperature and holding time on the properties of 3Y-ZrO_2 microfiltration membranes. *J. Mat. Sci.*, 2001, **36**, 3437–3446.
15. Shinohara, N., Okumiya, M., Hotta, T., Nakahira, K. and Naito, M., Morphological changes in process-related large pores of granular compacted and sintered alumina. *J. Am. Ceram. Soc.*, 2000, **83**, 1633–1640.
16. Leofanti, G., Padovan, M., Tozzola, G. and Venturelli, B., Surface area and pore texture of catalysts. *Catalysis Today*, 1998, **41**, 207–219.
17. Do, D. D., *Adsorption Analysis: Equilibria and Kinetics*. Imperial College Press, 1998, pp. 397–398.